LOCALIZATION OF FAST MOBILE ROBOTS BASED ON AN ADVANCED ANGLE-MEASUREMENT TECHNIQUE

U.D. Hanebeck and G. Schmidt

Department for Automatic Control Engineering, Technische Universität München, 80290 München, Germany
((hnb,gs)@lsr.e-technik.tu-muenchen.de)

(Received November 1995; in final form June 1996)

Abstract. This paper is concerned with the absolute localization of mobile robots, which are equipped with an onboard device performing angular measurements on the location of known but mutually indistinguishable landmarks. Novel algorithms are proposed, 1. for efficient posture initialization based on a simple *linear* solution scheme, and 2. for purposes of recursive posture estimation. Derived within a set–theoretic framework, the algorithms cope with nonwhite, non–Gaussian noise and deterministic errors. A typical application, localizing a floor–inspection robot on a long–range inspection mission, is used to demonstrate the implementation and performance of the proposed posture estimator.

Keywords. Angular measurements; nonlinear filtering; recursive estimation; set theory; vehicles

1. INTRODUCTION

This paper introduces a new approach to estimating the absolute posture, i.e., position x, y, orientation ψ, of a fast mobile robot on a planar surface. The estimation is based upon onboard measurements of angular locations of known landmarks. Both initialization of the robot posture and recursive in–motion posture estimation are considered.

For initialization purposes, a set of angles measured with respect to the robot's coordinate system needs to be paired with a subset of the mutually indistinguishable landmarks that are extracted from a map. In (Wiklund, *et al.*, 1988), an enumerative scheme has been reported for pairing the first three angles with landmarks. The remaining angles are used for plausibility tests. Several solutions for calculating the posture, given the association of measured angles with landmarks have been reported: Wiklund, *et al.* (1988), Sutherland and Thompson (1994), and Tsumura, *et al.* (1993) consider only triples of landmarks. For the case of more than three landmarks some authors average triple solutions, while others use iterative techniques. Betke and Gurvits (1994) supply a closed–form solution for N angles without considering uncertainties. In this paper, an efficient association algorithm is developed. The algorithm discards false measurements, it is fast, and it is further accelerated by incorporating prior knowledge. In addition, the algorithm takes advantage of a simple closed–form solution, which consists of a set of $N-1$ *linear* equations for the vehicle position, see Section 3. An error–propagation analysis considers uncertainties in both landmark positions and angle measurement.

Posture estimates are sequentially updated by newly incoming angle measurements, if the vehicle's velocity is high compared to the angle measurement rate. The updates are usually performed within the Kalman filtering framework. White Gaussian zero-mean random processes are then used as uncertainty models. In (Wiklund, *et al.*, 1988), a Kalman filtering scheme is introduced for this purpose, based on a kinematic vehicle model; fusion of dead–reckoning information is not considered. Nishizawa, *et al.* (1995) use a Kalman filter to fuse sensor data with dead–reckoning data. Real–world uncertainties, however, also include non–Gaussian, nonwhite noise and systematic errors. These uncertainties may easily be con-

sidered in a set–theoretic setting. For example, Atiya and Hager (1993) describe a set–theoretic approach to stereo–vision based robot localization without dead–reckoning. In this paper, a solution is given to the problem of locating a mobile robot based on dead–reckoning and onboard angle measurements in a set–theoretic framework (see Section 4). Basic concepts for prediction, measurement, data validation, and combination of information are developed from a set–theoretic viewpoint in Sections 4.1 to 4.4. Section 4.4 then discusses two new approaches, for tailoring set–theoretic estimators to specific applications, and for achieving robustness against modeling errors. The individual components are tied together in Section 4.5 to construct a recursive set–theoretic estimator with real–time capabilities. Combining set–theoretic and Bayesian estimation is discussed in (Hanebeck, *et al.*, 1996).

The proposed localization scheme may be applied to any mobile robot which is equipped with an onboard angle measurement device. Angle–measurement devices are common in mobile robot applications, since they are readily available, simple, and inexpensive. For validating the proposed localization scheme, a mobile robot equipped with a laser–based angle–measurement system is used. The angle–measurement system is employed for high–accuracy navigation and serves as a reference sensor for the development of other sensors. In this paper, a specific application for high–accuracy navigation is studied: localizing a floor–inspection robot on long–range inspection missions. Experimental results are presented in detail in Section 5 to assess the performance of the proposed posture–estimation scheme.

2. PROBLEM FORMULATION

Consider a pool of M landmarks in a two–dimensional world or map. The positions of the landmarks $\underline{x}_i^{\mathrm{LM}} = [x_i^{\mathrm{LM}}, y_i^{\mathrm{LM}}]^T$, $i = 0, 1, \ldots, M-1$ in a reference coordinate system are assumed to be known with additive bias errors $\underline{\Delta}_i^{\mathrm{LM}} = [\Delta x_i^{\mathrm{LM}}, \Delta y_i^{\mathrm{LM}}]^T$, which are of course unknown. True values of $*$ are denoted as $\tilde{*}$, nominal values as $\hat{*}$. The true landmark position $\tilde{\underline{x}}_i^{\mathrm{LM}}$ is assumed to be somewhere within the set

$$\Omega_i^{\mathrm{LM}} = \{\underline{x}_i^{\mathrm{LM}} : \underline{x}_i^{\mathrm{LM}} = \hat{\underline{x}}_i^{\mathrm{LM}} + \underline{\Delta}_i^{\mathrm{LM}},\ \underline{\Delta}_i^{\mathrm{LM}} \in \Omega_i^{\Delta}\}\ , \tag{1}$$

where the errors in the position of landmark i are confined to an ellipsoidal set Ω_i^{Δ} given by

$$\Omega_i^{\Delta} = \{\underline{\Delta}_i^{\mathrm{LM}} : (\underline{\Delta}_i^{\mathrm{LM}})^T (\mathbf{C}_i^{\mathrm{LM}})^{-1} \underline{\Delta}_i^{\mathrm{LM}} \leq 1\}\ . \tag{2}$$

The robot has the capability to determine the angular locations of these landmarks with respect to its coordinate system. Individual landmarks do not necessarily have to be distinguished from one another. The angle measurements are corrupted by additive noise, i.e., $\hat{\alpha}_i = \tilde{\alpha}_i + \Delta\alpha_i$, where $\Delta\alpha_i$ is assumed to be bounded in amplitude (b.i.a.) according to $|\Delta\alpha_i| < \delta_i^{\alpha}$. To account for possible occlusion of landmarks in nonconvex rooms, partitioning walls are added to the map. The landmarks are ordered in the map in such a way that the robot always detects the subset of unoccluded landmarks in that order when scanning counter–clockwise.

3. POSTURE INITIALIZATION

This section is concerned with (re–)initializing the robot posture $\underline{x} = [x, y, \psi]^T$ in nonconvex rooms, when only very little prior knowledge of the robot posture is available. A priori information is specified by confining the posture to an ellipsoidal set $\Omega_{\mathrm{a\ priori}}$. M landmarks are available and $N > 3$ angles α_i, $i = 0, 1, \ldots, N-1$ have been measured. The association, i.e., the list of pairings of measured angles to landmarks, is initially unknown. Inspired by the interpretation–tree (IT) method in (Drumheller, 1987), the association search is kept from becoming intractable by approaching it in two steps: in the first step, for every measured angle α_i the set of visible landmarks from $\Omega_{\mathrm{a\ priori}}$ is determined. In the second step, these visibility constraints are exploited for pruning the IT. Thus, only a small portion of all associations needs to be generated and tested.

Step 1: The projection of $\Omega_{\mathrm{a\ priori}}$ onto the x/y-plane is examined at polar grid points $x(r,\theta)$, $y(r,\theta)$ for some r, θ. A visibility matrix $\mathcal{V}$ is defined, with dimensions N by M. The elements $\mathcal{V}_{ij}$ are Boolean variables which are TRUE, if the single measured angle α_i may be caused by landmark j. A visibility test is performed for every grid point $x(r,\theta)$, $y(r,\theta)$. If the landmark j is visible, i.e., when the straight line from the grid point $x(r,\theta)$, $y(r,\theta)$ to x_j^{LM}, y_j^{LM} does not intersect any partitioning walls, a hypothetical angle α^{hyp} is calculated. The minimum and maximum angles at $x(r,\theta)$, $y(r,\theta)$ within $\Omega_{\mathrm{a\ priori}}$ are denoted as ψ_{LOW}, ψ_{HIGH} respectively. α_i may then be caused by landmark j, if $\alpha_i + \psi_{\mathrm{LOW}} < \alpha^{\mathrm{hyp}} < \alpha_i + \psi_{\mathrm{HIGH}}$. If row i of $\mathcal{V}$ does not contain any TRUE value, α_i has been identified as a false measurement. Row i is then removed from $\mathcal{V}$, and the number of measurements N is decremented.

Step 2: Only those candidate associations are generated that do not violate the visibility constraints represented by $\mathcal{V}$, and that also follow the ordering assumption. Erroneous measurements are handled efficiently by adopting the "least bad data" constraint proposed in (Grimson and Lozano-Pérez, 1985). For a specific associa-

tion, a tentative position is calculated and checked for compatibility with the error bounds, the posture constraint $\Omega_{\text{a priori}}$, and the requirements for joint visibility of all landmarks involved.

Tentative postures are quickly calculated by the use of a closed–form solution. The corresponding set of $N-1$ *linear* equations for the position is derived next. The measurement equation for a single angle measurement α_i is given by

$$\alpha_i = \operatorname{atan2}(x_i^{\mathrm{LM}} - x, y_i^{\mathrm{LM}} - y) - \psi \ , \qquad (3)$$

$i = 0, 1, \ldots, N-1$. Define γ_i as the difference between two consecutive angle measurements α_i and α_{i+1}, $\gamma_i = \alpha_{i+1} - \alpha_i$. It follows that

$$\tan(\gamma_i) = \frac{\frac{y_{i+1}^{\mathrm{LM}}-y}{x_{i+1}^{\mathrm{LM}}-x} - \frac{y_i^{\mathrm{LM}}-y}{x_i^{\mathrm{LM}}-x}}{1 + \frac{y_{i+1}^{\mathrm{LM}}-y}{x_{i+1}^{\mathrm{LM}}-x} \cdot \frac{y_i^{\mathrm{LM}}-y}{x_i^{\mathrm{LM}}-x}} \ , \qquad (4)$$

which may be rewritten as

$$\begin{aligned} & y_{i+1}^{\mathrm{LM}} y_i^{\mathrm{LM}} + x_{i+1}^{\mathrm{LM}} x_i^{\mathrm{LM}} + \cot(\gamma_i)\{x_{i+1}^{\mathrm{LM}} y_i^{\mathrm{LM}} - y_{i+1}^{\mathrm{LM}} x_i^{\mathrm{LM}}\} \\ &= \begin{bmatrix} \cot(\gamma_i)\{y_i^{\mathrm{LM}} - y_{i+1}^{\mathrm{LM}}\} + x_{i+1}^{\mathrm{LM}} + x_i^{\mathrm{LM}} \\ \cot(\gamma_i)\{x_{i+1}^{\mathrm{LM}} - x_i^{\mathrm{LM}}\} + y_{i+1}^{\mathrm{LM}} + y_i^{\mathrm{LM}} \end{bmatrix}^T \begin{bmatrix} x \\ y \end{bmatrix} \\ & \qquad - \begin{bmatrix} x & y \end{bmatrix} \begin{bmatrix} x \\ y \end{bmatrix} \end{aligned} \qquad (5)$$

for $i = 0, \ldots, N-1$. Index operations are performed modulo N, i.e., $i+1 = 0$ for $i = N-1$. After some manipulations (Hanebeck and Schmidt, 1996), a system of $N-1$ equations that are *linear* in x and y is obtained as

$$\underline{z} = \mathbf{H}\,[x, y]^T + \underline{e} \qquad (6)$$

with

$$\begin{aligned} \underline{z} &= [z_0, z_1, \ldots, z_{N-2}]^T \\ \mathbf{H} &= [\underline{h}_0, \underline{h}_1, \ldots, \underline{h}_{N-2}]^T \\ \underline{h}_i &= [h_i^x, h_i^y]^T \end{aligned} \qquad (7)$$

and error $\underline{e} = [e_0, e_1, \ldots, e_{N-2}]^T$. The corresponding elements are given by

$$\begin{aligned} z_i = & \cos(\gamma_i)\sin(\gamma_{i+1})\{x_{i+1}^{\mathrm{LM}} y_i^{\mathrm{LM}} - y_{i+1}^{\mathrm{LM}} x_i^{\mathrm{LM}}\} \\ & + \sin(\gamma_i)\sin(\gamma_{i+1})\{x_{i+1}^{\mathrm{LM}} x_i^{\mathrm{LM}} - x_{i+2}^{\mathrm{LM}} x_{i+1}^{\mathrm{LM}} \\ & \qquad + y_{i+1}^{\mathrm{LM}} y_i^{\mathrm{LM}} - y_{i+2}^{\mathrm{LM}} y_{i+1}^{\mathrm{LM}}\} \\ & - \sin(\gamma_i)\cos(\gamma_{i+1})\{x_{i+2}^{\mathrm{LM}} y_{i+1}^{\mathrm{LM}} - y_{i+2}^{\mathrm{LM}} x_{i+1}^{\mathrm{LM}}\} \end{aligned}$$

$$\begin{aligned} h_i^x = & \cos(\gamma_i)\sin(\gamma_{i+1})\{y_i^{\mathrm{LM}} - y_{i+1}^{\mathrm{LM}}\} \\ & + \sin(\gamma_i)\sin(\gamma_{i+1})\{x_i^{\mathrm{LM}} - x_{i+2}^{\mathrm{LM}}\} \\ & - \sin(\gamma_i)\cos(\gamma_{i+1})\{y_{i+1}^{\mathrm{LM}} - y_{i+2}^{\mathrm{LM}}\} \end{aligned} \qquad (8)$$

$$\begin{aligned} h_i^y = & \cos(\gamma_i)\sin(\gamma_{i+1})\{x_{i+1}^{\mathrm{LM}} - x_i^{\mathrm{LM}}\} \\ & + \sin(\gamma_i)\sin(\gamma_{i+1})\{y_i^{\mathrm{LM}} - y_{i+2}^{\mathrm{LM}}\} \\ & - \sin(\gamma_i)\cos(\gamma_{i+1})\{x_{i+2}^{\mathrm{LM}} - x_{i+1}^{\mathrm{LM}}\} \ , \end{aligned}$$

for $i = 0, \ldots, N-2$. An error–propagation analysis is performed, which provides: 1. the optimal weighting matrix for the LS–solution of (6) and 2. the initial set of postures that are compatible with the a priori error bounds. This analysis is found elsewhere. Once x and y are known, ψ can be obtained as the (weighted) LS–solution of (3) for $i = 0, 1, \ldots, N-1$.

4. RECURSIVE IN–MOTION LOCALIZATION

Once the robot posture is initialized using the method developed in the last section, the robot starts moving. During motion, the robot posture estimate is updated with the information obtained from every additional angle measurement. Dead–reckoning data is used to smooth the estimate by predicting the posture change between two measurements.

Usually, problems of this type are solved within the Kalman filter framework. Measurement noise and dead–reckoning errors are assumed to be zero–mean, white, mutually independent random processes. For these assumptions, the Kalman prediction step (time update) provides first– and second–order moments of the predicted state, given *any* noise distribution. The Kalman estimation step (measurement update), however, yields precise values of first– and second–order moments of the estimated state only for Gaussian noise densities. For other noise densities, the Kalman estimation step just provides the best *linear* estimator.

In realistic applications, however, a state estimator must cope with 1. non–Gaussian noise, 2. nonwhite noise, 3. systematic errors, and 4. mutally dependent noise sources. For the localization problem at hand, at least two error sources may be identified that violate the Kalman filter assumptions:

1. landmark positions are only known with a deterministic offset, and
2. a robot's dead–reckoning system — especially for the omnidirectional robot considered in Section 5 — suffers from nonwhite noise and deterministic errors.

A nonlinear filter, which copes with the above mentioned uncertainties, is developed by set–theoretic considerations below. The proposed filter is first–order for the sake of simplicity, i.e, strictly optimal for white b.i.a. noise processes. However, the output represents an upper bound for nonwhite noise or deterministic errors, which is in sharp contrast to first–order Kalman filters. Furthermore, the noise processes may stem from *any* distribution that is compatible with the amplitude bounds.[1] Ellipsoidal bounding sets (EBS) are used to approximate the sets of feasible solutions. These sets may be manipulated by matrix operations only, and thus result in efficient algorithms with real–time capabilities.

[1] Not only uniform densities !

Section 4.1 develops a simple method for set–theoretic posture prediction. Measured angles are associated with landmarks in Section 4.2. The determination of the set of feasible postures defined by a single angle measurement is discussed in Section 4.3. An efficient algorithm for approximating the intersection of the prediction and measurement sets is introduced in Section 4.4. The filtering components are put together in Section 4.5 to form a nonlinear recursive set–theoretic estimator.

4.1 *Set–theoretic Posture Prediction*

When moving from one measurement at time $k-1$ to the next, the estimate of the vehicle's posture suffers from accumulating uncertainties. The relative uncertainty may be estimated and must then be "added" to the absolute uncertainty prevalent at time $k-1$. Usually, the relative uncertainty is assumed to be independent from the absolute uncertainty at time $k-1$, which leads to the well known Kalman covariance propagation formula. For nonwhite noise and deterministic errors, however, this propagation formula is too optimistic. In the following, a simple set–theoretic propagation formula is developed, that provides a guaranteed upper bound for the posture error, even in the case of nonwhite and deterministic errors.

The result of the fusion process at time $k-1$ is denoted as Ω^E_{k-1} and given by

$$\Omega^E_{k-1} = \{\underline{x}^E_{k-1} : (\underline{x}^E_{k-1} - \hat{\underline{x}}^E_{k-1})^T \left(\mathbf{C}^E_{k-1}\right)^{-1} (\underline{x}^E_{k-1} - \hat{\underline{x}}^E_{k-1}) \leq 1\}. \tag{9}$$

The dead–reckoning system supplies the set of relative postures with respect to Ω^E_{k-1}, henceforth denoted as

$$\Omega^\Delta_k = \{\underline{x}^\Delta_k : (\underline{x}^\Delta_k - \hat{\underline{x}}^\Delta_k)^T \left(\mathbf{C}^\Delta_k\right)^{-1} (\underline{x}^\Delta_k - \hat{\underline{x}}^\Delta_k) \leq 1\} . \tag{10}$$

The calculation of Ω^Δ_k depends on the vehicle kinematic. For the omnidirectional vehicle considered in Section 5, determination of Ω^Δ_k is rather complex and outside the scope of this paper.

The exact set of absolute postures is given by transforming the set Ω^Δ_k to the inertial coordinate system for all feasible posture estimates contained in Ω^E_{k-1}. This is written as

$$\Omega^P_k = \{\underline{x}^P_k : \underline{x}^P_k = \mathbf{I}\,\underline{x}^E_{k-1} + \mathbf{B}_k\,\underline{x}^\Delta_k\} , \tag{11}$$

with $\underline{x}^E_{k-1} \in \Omega^E_{k-1}$, $\underline{x}^\Delta_k \in \Omega^\Delta_k$, $\mathbf{I}$ the identity matrix, and

$$\mathbf{B}_k = \begin{bmatrix} \cos(\psi^E_{k-1}) & -\sin(\psi^E_{k-1}) & 0 \\ \sin(\psi^E_{k-1}) & \cos(\psi^E_{k-1}) & 0 \\ 0 & 0 & 1 \end{bmatrix} . \tag{12}$$

Unfortunately, Ω^P_k is not in general an ellipsoid. Linearizing (11) around the nominal values yields

$$\underline{x}^P_k - \hat{\underline{x}}^P_k \approx \mathbf{J}^E_k(\underline{x}^E_{k-1} - \hat{\underline{x}}^E_k) + \hat{\mathbf{B}}_k(\underline{x}^\Delta_k - \hat{\underline{x}}^\Delta_k) \tag{13}$$

with the Jacobian given by

$$\mathbf{J}^E_k = \begin{bmatrix} 1 & 0 & -(\hat{y}^P_k - \hat{y}^E_{k-1}) \\ 0 & 1 & (\hat{x}^P_k - \hat{x}^E_{k-1}) \\ 0 & 0 & 1 \end{bmatrix} . \tag{14}$$

Ω^P_k may then be approximated as the EBS for the Minkowski sum of the two ellipsoids in (13)

$$\Omega^P_k \approx \{\underline{x}^P_k : (\underline{x}^P_k - \hat{\underline{x}}^P_k)^T \left(\mathbf{C}^P_k\right)^{-1} (\underline{x}^P_k - \hat{\underline{x}}^P_k) \leq 1\} , \tag{15}$$

with center

$$\hat{\underline{x}}^P_k = \mathbf{I}\,\hat{\underline{x}}^E_{k-1} + \hat{\mathbf{B}}_k\,\hat{\underline{x}}^\Delta_k \tag{16}$$

and

$$\mathbf{C}^P_k = \frac{\Xi_k}{0.5-\kappa} + \frac{\Gamma_k}{0.5+\kappa} , \tag{17}$$

with $\Xi_k = \mathbf{J}^E_k \mathbf{C}^E_{k-1} (\mathbf{J}^E_k)^T$, $\Gamma_k = \hat{\mathbf{B}}_k \mathbf{C}^\Delta_k \hat{\mathbf{B}}^T_k$, for $-0.5 < \kappa < 0.5$.[2] κ may be selected such that a measure of the "size" of Ω^P_k is minimized.

4.2 *Association of Angles with Landmarks*

The set of predicted postures Ω^P_k is used to extract potentially visible landmarks from the map and to calculate validation bounds for the angles to each of these landmarks. The subset of potentially visible landmarks is given by those L landmarks that are not occluded by a priori known objects. The hypothetical angles to these landmarks with respect to the vehicle coordinate system are given by

$${}^{(i)}\alpha^{\text{hyp}}_k = \text{atan2}(x^{\text{LM}}_i - x^P_k, y^{\text{LM}}_i - y^P_k) - \psi^P_k , \tag{18}$$

for $i = 0, \ldots, L-1$. An angle α_k measured at time k is associated with the landmark that produces the smallest deviation between hypothesized and measured angles. If this deviation is larger than a prespecified bound, the measured angle is discarded.

4.3 *Posture Set Defined by Measurements*

The measurement equation for a single α_k at time k and an associated landmark at $\underline{x}^{\text{LM}}$ is given by (3). It may be rewritten to yield the exact set of

[2] $-0.5 < \kappa < 0.5$ leads to symmetric solution formulae for κ in contrast to the formulation in (Schweppe, 1973), that assumes $0 < \kappa < 1$.

all vehicle postures compatible with the measured angle. The set is given by

$$\Omega_k^M = \{\underline{x}_k^M : \sin(\alpha_k + \psi_k^M)\{x^{\mathrm{LM}} - x_k^M\} = \cos(\alpha_k + \psi_k^M)\{y^{\mathrm{LM}} - y_k^M\}, \; |\alpha_k - \hat{\alpha}_k| < \delta^\alpha \,,\; \underline{x}^{\mathrm{LM}} \in \Omega^{\mathrm{LM}}\} \quad (19)$$

Linearizing around the predicted posture $\hat{\underline{x}}_k^P$, the measured angle $\hat{\alpha}_k$, and the nominal landmark position $\hat{\underline{x}}^{\mathrm{LM}}$ yields an approximation of the set of all vehicle postures defined by the measurement

$$\Omega_k^M \approx \{\underline{x}_k^M : z_k = \underline{H}_k^T \underline{x}_k^M + e_k \,,\; e_k^2 \le E_k\} \;. \quad (20)$$

z_k, $\underline{H}_k$, and E_k are given in (Hanebeck and Schmidt, 1996).

4.4 *Combination of Data*

After measurement k, the vehicle posture simultaneously belongs to two sets: 1. the prediction set Ω_k^P, which carries all past information from dead-reckoning and previous measurements, and 2. the measurement set Ω_k^M, which accounts for the last angle measurement. Consequently, fusion consists of calculating the intersection of the two sets Ω_k^P, Ω_k^M. However, the intersection of Ω_k^P and Ω_k^M is, again, not in general an ellipsoid. Thus, an ellipsoid circumscribing the intersection is required to arrive at a recursive scheme. A bounding ellipsoid is given by (Sabater and Thomas, 1991)

$$\begin{aligned}
\Omega_k^E &= \{\underline{x}_k^E : (\underline{x}_k^E - \hat{\underline{x}}_k^E)\left(\mathbf{C}_k^E\right)^{-1}(\underline{x}_k^E - \hat{\underline{x}}_k^E)^T \le 1\} \\
\mathbf{C}_k^E &= d_k \mathbf{D}_k \\
\mathbf{D}_k &= \mathbf{C}_k^P - \lambda_k \frac{\mathbf{C}_k^P \underline{H}_k \underline{H}_k^T \mathbf{C}_k^P}{E_k + \lambda_k G_k} \\
\hat{\underline{x}}_k^E &= \hat{\underline{x}}_k^P + \lambda_k \mathbf{D}_k \underline{H}_k E_k^{-1} \epsilon_k \\
\epsilon_k &= z_k - \underline{H}_k^T \hat{\underline{x}}_k^P \\
G_k &= \underline{H}_k^T \mathbf{C}_k^P \underline{H}_k \\
d_k &= 1 + \lambda_k - \lambda_k \epsilon_k^2 / (E_k + \lambda_k G_k)
\end{aligned} \quad (21)$$

for all $\lambda_k \ge 0$. The set Ω_k^E possesses the interesting property that it both contains the intersection of the measurement and the prediction set and is itself contained in their union, i.e.,

$$(\Omega_k^M \cap \Omega_k^P) \subset \Omega_k^E \subset (\Omega_k^M \cup \Omega_k^P) \;. \quad (22)$$

Furthermore, the set Ω_k^E is valid for any noise distribution complying with the amplitude bounds. But more importantly, no independence assumption is used in the derivation. As a result, the estimator provides a reliable uncertainty quantification, even in the case of nonwhite and deterministic measurement errors.

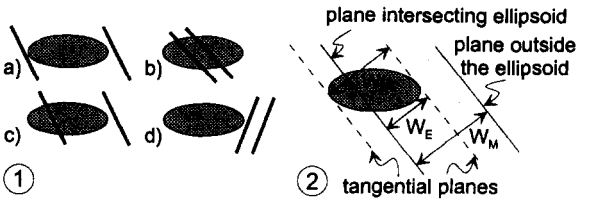

Fig. 1. 1: Configurations for measurement strip Ω_k^M (20) and prediction ellipsoid Ω_k^P (two-dimensional visualization). 2: Definitions for assessing consistency of the sets Ω_k^M, Ω_k^P.

Although very similar in appearance to the Kalman filter equations [3], (21) defines a nonlinear estimator which inherits a selective update mechanism. The nonlinear estimator comprises the following cases:

- **Consistency:** Prediction set Ω_k^P and measurement set Ω_k^M possess common points.
  - **Full consistency:**
    No uncertainty reduction: The actual measurement is of no help in reducing the uncertainty, Fig 1.1 a).
    Uncertainty reduction: Both planes defining the measurement set intersect the ellipsoidal prediction set, Fig. 1.1 b).
  - **Partial consistency:** Only one plane intersects the prediction set, Fig. 1.1 c).
- **Inconsistency:** Prediction set Ω_k^P and measurement set Ω_k^M do not share a common point, Fig. 1.1 d).

Inconsistency is detected by checking the condition

$$d_k(\lambda_k^{\min}) < 0 \;, \quad \text{with } \lambda_k^{\min} = \sqrt{\frac{E_k}{G_k}} \;. \quad (23)$$

No update is then performed. For the case of **consistency** of ellipsoid and strip, the *volume* of the bounding ellipsoid in (21) may be minimized by selecting the weight λ_k^{OPT} as the most positive root of the quadratic equation given by (Sabater and Thomas, 1991)

$$\begin{aligned}
&\lambda_k^2 (N-1) G_k^2 + \lambda_k \{\epsilon_k^2 + (2N-1)E_k - G_k\} G_k \\
&+ \{N(E_k - \epsilon_k^2) - G_k\} E_k = 0 \;,
\end{aligned} \quad (24)$$

where N is the dimension; here $N = 3$. The case of **no uncertainty reduction** is characterized by $\lambda_k^{\mathrm{OPT}} \le 0$.

Ellipsoidal Bounding Set with Minimum Volume Projection Onto Subspace. For the application considered here, it is more natural to minimize the volume of the projection of the EBS onto the x, y subspace. The EBS with a *minimum-volume*

[3] In fact, for $\lambda_k = 1$ and $d_k = 1$, (21) yields the Kalman filter equations, when $\mathbf{C}_k^E$, $\mathbf{C}_k^P$, and E_k are interpreted as covariance matrices.

projection onto an arbitrary subspace is obtained with λ_k^{OPT} as the positive real root of

$$\begin{aligned}&\lambda_k^3(G_k - K_k)G_k^2 L\\ &+\lambda_k^2\{L(3G_k - 2K_k) - K_k\}E_k G_k\\ &+\lambda_k\{\epsilon_k^2(L(K_k - G_k) + K_k)\\ &\quad +E_k(L(3G_k - K_k) - K_k) - G_k K_k\}E_k\\ &+\{L(E_k - \epsilon_k^2) - K_k\}E_k^2 = 0\ ,\end{aligned} \tag{25}$$

with L the subspace dimension and

$$K_k = \underline{H}_k^T(\bar{\mathbf{C}}_k^P)^T[\mathrm{proj}(\mathbf{C}_k^P)]^{-1}\bar{\mathbf{C}}_k^P\underline{H}_k. \tag{26}$$

$\bar{\mathbf{C}}_k^P$ is obtained from $\mathbf{C}_k^P$ by eliminating the rows not associated with the subspace being considered. The proof is patterned after the one in (Deller and Luk, 1989) and is given in (Hanebeck and Schmidt, 1996). Application to the localization problem leads to a tailored bounding operation. The inherently high precision of the orientation estimate ψ_k^E compared to the position estimate x_k^E, y_k^E is considered by minimizing the projection of the EBS onto the x, y subspace. The resulting EBS is more conservative in ψ_k^E, but tight for the more critical position estimate x_k^E, y_k^E.

Robust Fusion. Using the "smallest" EBS is successful as long as the model is sufficiently precise. However, modeling errors may lead to an unrealistically small estimation set Ω_k^E. Enhanced robustness is achieved by imposing a higher priority on the set of predicted states Ω_k^P since it contains all past information. This priority should depend on the degree of consistency of the two sets Ω_k^P and Ω_k^M. Roughly speaking, the idea is to select the set Ω_k^E such that it exhibits a growing tendency towards the prediction set Ω_k^P with a falling degree of consistency of the sets Ω_k^P and Ω_k^M. Referring to Fig. 1.2, a reasonable consistency measure is given by the intersection width W_k^E divided by the geometric mean of the strip width W_k^M and the ellipsoid width W_k^P, i.e.,

$$\mathrm{CM}(\Omega_k^P, \Omega_k^M) = \frac{W_k^E}{\sqrt{W_k^P W_k^M}}\ ,\ 0 \le \mathrm{CM} \le 1\ . \tag{27}$$

λ_k in (21) is selected from $[0, \lambda_k^{\mathrm{OPT}}]$ as an appropriate function of the consistency measure. For this purpose, a shifted logistic function

$$\lambda_k = \lambda_k^{\mathrm{OPT}}/[1 + \exp(-S(\mathrm{CM} - M))], \tag{28}$$

is used with $S = 10$, $M = 0.5$. The influence of this extension to the fusion result is demonstrated in Fig. 2 by comparison with the common approach for four cases. For the common approach, the volume of the resulting EBS Ω_k^E experiences large changes when the measurement set just changes slightly. Single (unmodeled) measurement outliers may lead to an extremely small

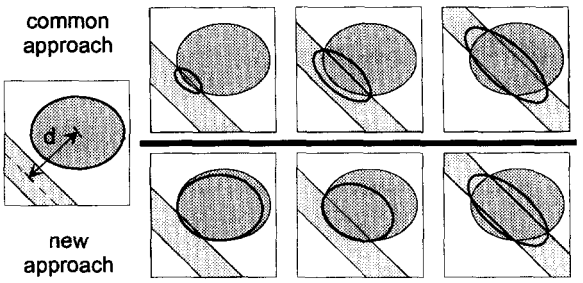

Fig. 2. EBSs for the intersection of ellipsoid and strip. Top: Common scheme. Bottom: Extension employing consistency measures.

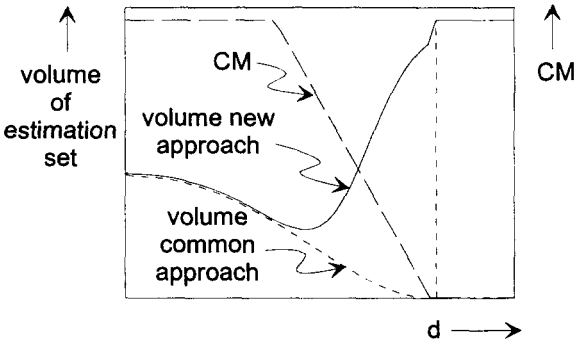

Fig. 3. Volume of the EBS in Fig. 2.

EBS. On the other hand, the new approach calculates Ω_k^E by modifying Ω_k^P depending on its consistency with Ω_k^M. Thus, single erroneous measurements have a reduced impact on the fusion result. The volume of the EBS as a function of d, where d is the distance of the ellipsoid center from the strip center axis, is shown for this example in Fig. 3.

Remark: The smallest possible EBS is obtained from (21) when both hyperplanes defining Ω_k^M intersect Ω_k^P. Overbounding occurs when one of the hyperplanes falls outside Ω_k^P. The minimum-volume bounding ellipsoid would then be obtained by parallel repositioning of the outside plane to be tangential to Ω_k^P (Cheung, *et al.*, 1993). This is not exploited here, since overbounding is intentionally performed in the case of partial consistency by using consistency measures.

4.5 *Set-theoretic Recursive Estimator*

The proposed recursive estimation scheme for localization during fast motion is depicted in Fig. 4. Based on the set of estimated postures Ω_{k-1}^E at time $k-1$, the visible landmarks are determined, and validation bounds for a measured angle are predicted. If the actual measured angle falls outside these bounds, it is discarded. Otherwise, it is associated with the best matching landmark and the measurement strip Ω_k^M is calculated. Ω_k^M is then fused with the set of predicted postures Ω_k^P to produce Ω_k^E. The feedback of $\underline{\hat{x}}_k^E$ to the pro-

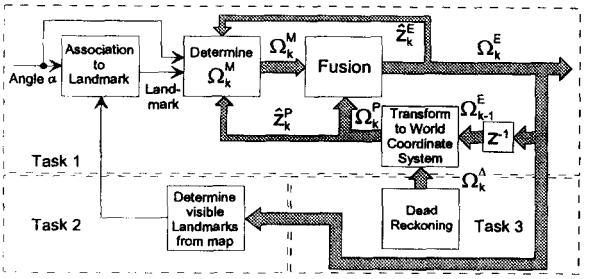

Fig. 4. Scheme of the set–theoretic recursive estimator.

cess for determination of Ω_k^M deserves some attention. $\hat{\underline{x}}_k^E$ replaces $\hat{\underline{x}}_k^P$ for iterative refinement of the linearization of (19). For implementation purposes, the scheme has been parallelized into three tasks: the fusion loop, the determination of landmarks not occluded by partitioning walls, and dead–reckoning.

5. EXPERIMENTAL VALIDATION

The performance of the new posture estimator is demonstrated by localizing a floor–inspection robot on a non–stop long–range mission. The inspection mission takes about 46 minutes and consists of covering a winding course of more than 1 km length. The nominal speed is about 1000 mm/sec. The floor–inspection robot is emulated by the general–purpose service robot ROMAN (Hanebeck and Schmidt, 1995) shown in Fig. 5. ROMAN is a full–scale mobile robot adapted to indoor requirements: width 0.63 m x depth 0.64 m x height 1.8 m. Three independently steerable wheel systems provide excellent maneuverability. Wheel diameters of 0.2 m allow travel across rough surfaces like carpeted floor. For absolute localization of ROMAN, an onboard laser–based goniometer is used. An eye–safe laser beam scans the environment in a horizontal plane and determines the azimuth angles to known artificial landmarks, i.e., retro–reflecting tape strips attached to the walls. The landmarks are not coded and the system does not provide distance information. 20 horizontal 360° scans per second are performed; absolute measurement accuracy is about 0.02°. A map contains nominal positions of 11 identical landmarks. Landmark positions have been acquired by the robot itself during an exploration trip. The dead–reckoning system comprises the robot's odometer and a gyroscope. The odometer is based on the drive wheels' encoders, and suffers from error sources like imperfect wheel coordination and uncertain wheel/floor contact points. The gyroscope suffers from a slowly time–varying unknown offset. During the inspection mission, the robot has to follow the path shown in Fig. 6. This is automatically generated according to an approach described in (Hofner and Schmidt, 1995) and yields a floor coverage of about 83 %. The actual path driven by the vehicle is shown in Fig. 7, together with the area covered by the vehicle outline. The planned path and the actual path are in good accordance. To underline the long–term stability of the proposed localization scheme, the robot's posture is initialized only once, using the techniques described in Section 3. After initialization, the robot repetitively travels along the path, without stopping. After 12 loops, the total distance travelled is about 1056 m; the total time is 46 min. The number of sharp 180° turns is 132 and the number of 90° turns is 72. The nominal speed is 1000 mm/sec, and the average speed is 411 mm/sec. The localization estimate based on the fusion of goniometer data and dead–reckoning is compared with data from dead–reckoning only. For visualization purposes, the incremental posture changes given by odometer and gyroscope are integrated for every loop and plotted, 1. with respect to the starting position of the respective loop in Fig. 9, and 2. with respect to the initial posture in Fig. 10. The highly correlated nature of the accumulating dead–reckoning errors is obvious. On the other hand, the vehicle is kept accurately on track by means of the localization estimate as shown in Fig. 8. The maximum absolute deviation was found to be in the order of ±5 cm and ±1°. The actual translational and angular velocities of the vehicle are plotted over time in Figs 11 and 12 respectively. The robot slows down to about 150 mm/sec during the sharp turning

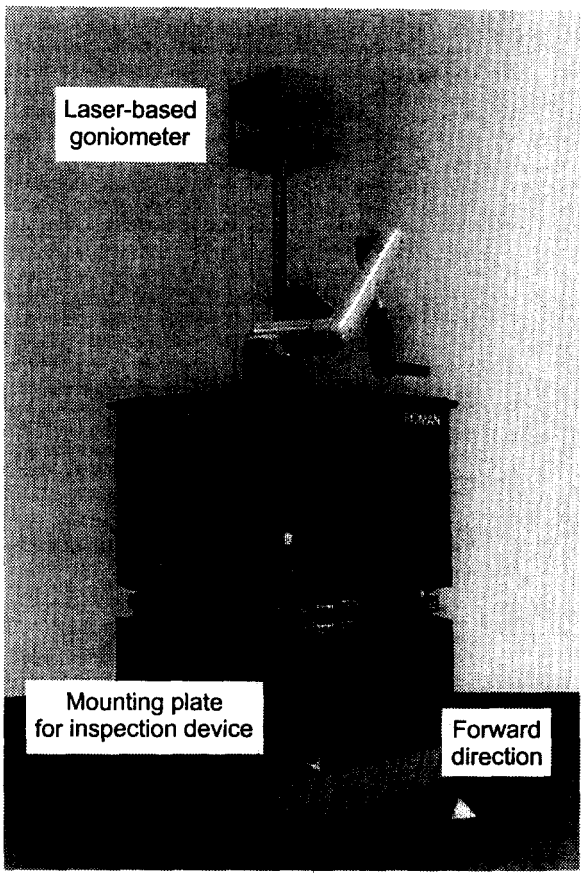

Fig. 5. Omnidirectional mobile service robot.

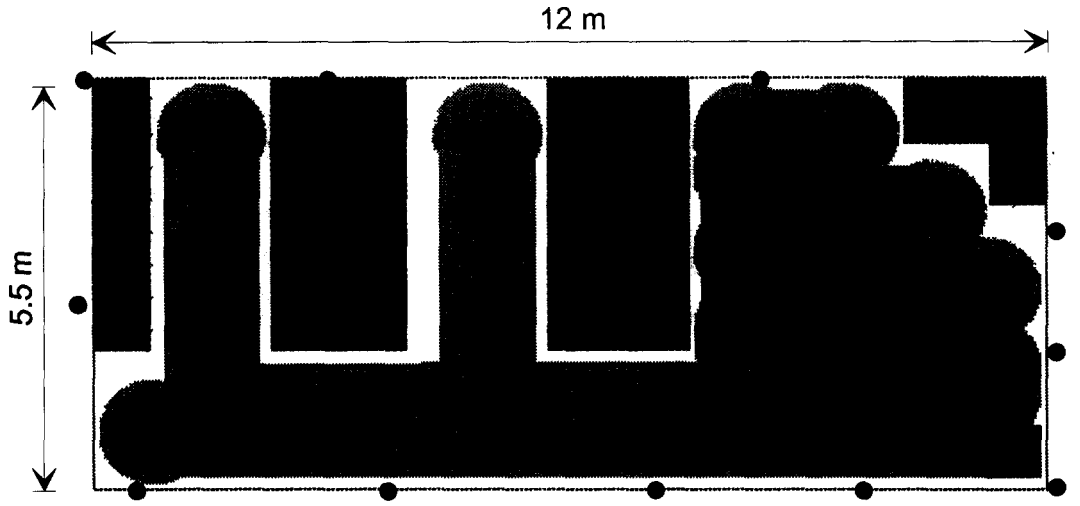

Fig. 6. Floor inspection mission: Planned path for complete floor coverage.

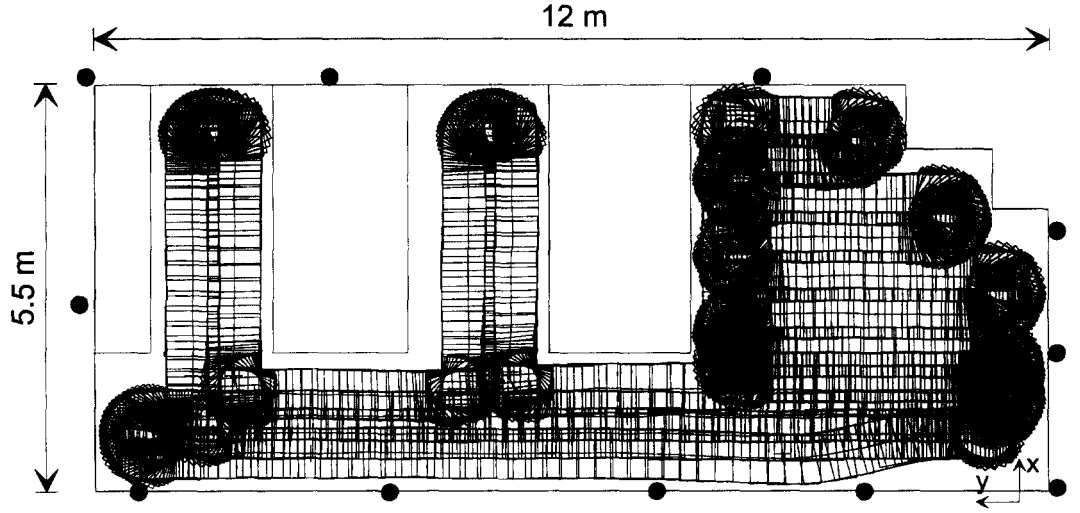

Fig. 7. Floor inspection mission: Actual path together with the area covered by the vehicle.

maneuvers and accelerates to a nominal speed of about 1000 mm/sec along the straight path segments. Of course, for the short path segments the robot slows down before arriving at the nominal speed. The angle measurements collected during the 46–minute mission are processed, with the results shown below.

update of robot posture estimate	Ω_k^M and Ω_k^P fully or partially consistent (Fig. 1.1 b, Fig. 1.1 c).	73.4 %
no update of robot posture estimate	no angle available, no landmark associated	7.85 %
	Ω_k^M and Ω_k^P inconsistent (Fig. 1.1 d).	4.75 %
	redundant information (Fig. 1.1 a).	14.00 %

In contrast to linear filters, the nonlinear filter defined by (21) does not incorporate redundant information. Furthermore, the ability to discard inconsistent information is inherent in the nonlinear filter. No additional consistency check is required. As a by–product, the selective update mechanism saves some computations.

The localization system has been in operation for more than one year, and serves as the basis for research on mobile manipulation tasks. It has been extensively tested by covering a distance of more than a hundred kilometers. Experiments include long–range navigation as discussed above, door opening/passing maneuvers, and high–speed runs with maximum velocities of up to 2 m/sec. Set–theoretic estimation proved to be an appropriate alternative to the common statistical approaches when dealing with strongly correlated or deterministic uncertainties.

6. CONCLUSION

Set–theoretic concepts have been applied to estimating the posture of fast–moving mobile robots which perform angular measurements on the location of known landmarks. The landmarks do not need to be distinguished by the robot. Four main results have been presented:

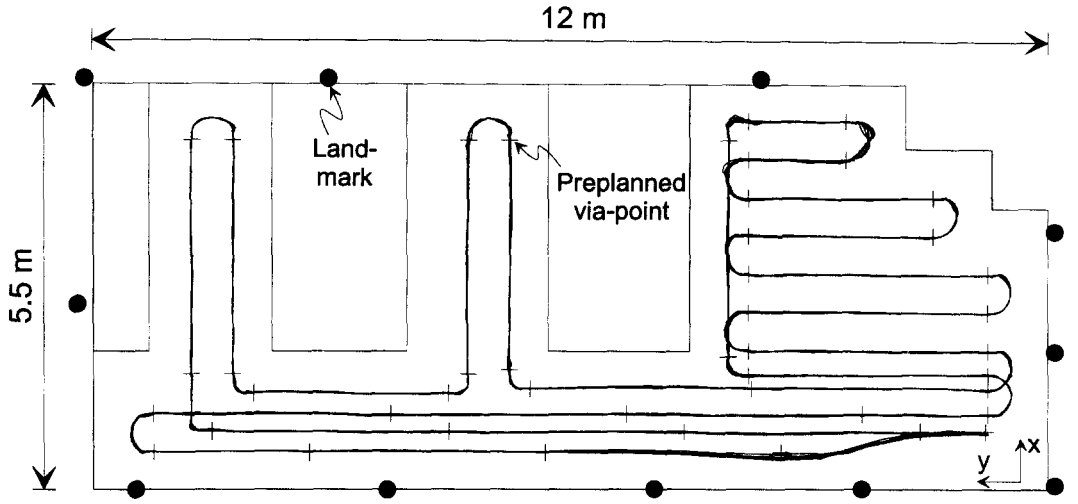

Fig. 8. Posture estimate for a total of 12 loops.

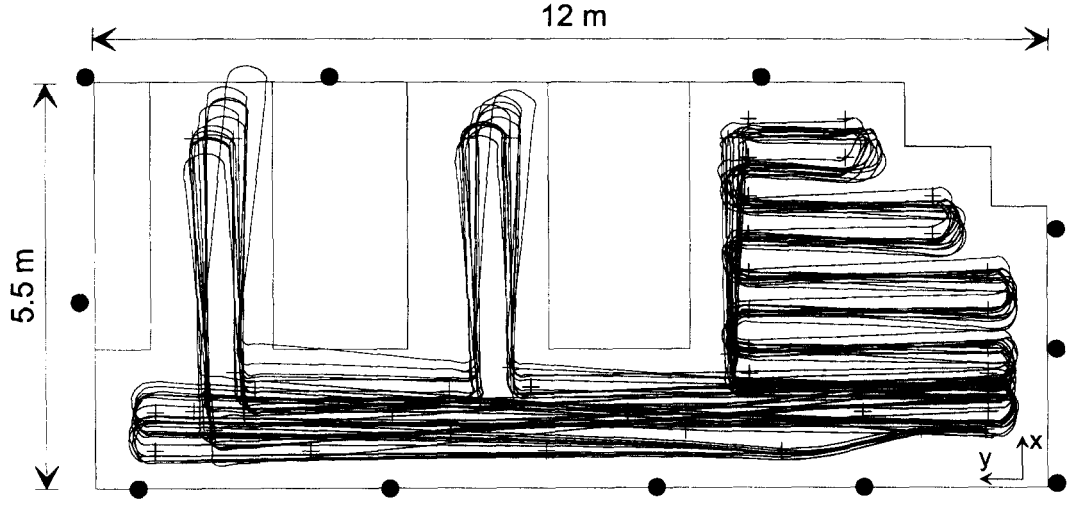

Fig. 9. Incremental posture changes given by dead–reckoning and gyroscope integrated with respect to the starting posture of the respective loop (total of 12 loops).

1. An efficient algorithm for posture initialization in nonconvex rooms,
2. a simple *closed–form* solution for the robot's position, given angular locations of N known landmarks, which consists of $N-1$ equations *linear* in the position,
3. an extension of the common minimum–volume EBS algorithms to obtain the EBS with *minimum–volume projection* onto an arbitrary subspace, and
4. a new design approach for set–theoretic estimators which employs consistency measures to achieve robustness against modeling errors.

The effectiveness of the proposed set–theoretic estimator has been demonstrated by experiments with a fast omnidirectional service robot. The full–scale robot is equipped with a laser–based goniometer which performs angular measurements on the location of tape strips attached to the wall and used as artificial landmarks. Localizing the robot on a long–range floor–inspection mission reveals a maximum deviation of about ± 5 cm and $\pm 1^0$ between true and estimated robot locations.

Acknowledgements

The work reported in this paper was supported by the Deutsche Forschungsgemeinschaft as part of an interdisciplinary research project on "Information Processing Techniques in Autonomous Mobile Robots" (SFB 331). The authors would like to thank W. Daxwanger and C. Hofner for valuable contributions to the planning and motion control scheme of ROMAN.

7. REFERENCES

Atiya, S. and G. D. Hager (1993). Real–Time Vision Based Robot Localization. *IEEE Trans. on Robotics and Automation* **9**(6), 785–800.

Betke, M. and L. Gurvits (1994). Mobile Robot Localization Using Landmarks. In: *Proc. of the 1994 IEEE/RSJ/GI Int. Conf. on Intelligent Robots and Systems, Munich, Germany.* pp. 135–142.

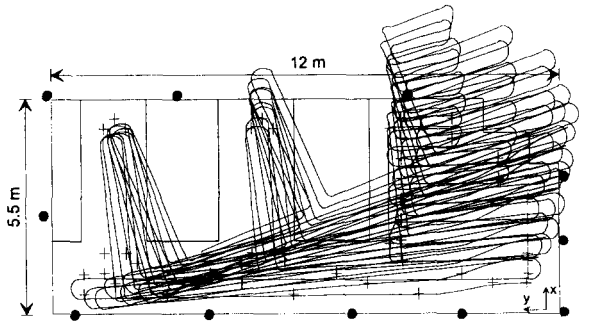

Fig. 10. Incremental posture changes given by dead–reckoning and gyroscope integrated with respect to the initial posture.

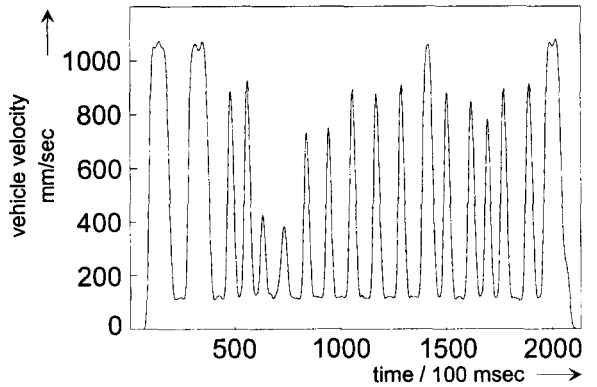

Fig. 11. Translational velocity of the vehicle for one loop of the path plotted in Fig. 6.

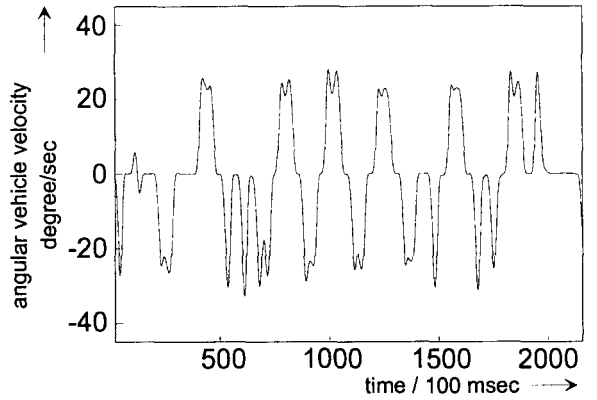

Fig. 12. Angular velocity of the vehicle for one loop of the path plotted in Fig. 6.

Cheung, M.-F., Yurkovich, S. and Passino, K. M. (1993). An Optimal Volume Ellipsoid Algorithm for Parameter Set Identification. *IEEE Trans. on AC* **38**(8), 1292–1296.

Deller, J. R. and T. C. Luk (1989). Linear Prediction Analysis of Speech Based on Set–Membership Theory. *Computer Speech and Language* **3**, 301–327.

Drumheller, M. (1987). Mobile Robot Localization Using Sonar. *IEEE Trans. on PAMI* **9**(2), 325–332.

Grimson, W. E. L. and T. Lozano-Pérez (1985). Recognition and Localization of Overlapping Parts From Sparse Data in Two and Three Dimensions. In: *Proc. of the 1985 IEEE Int. Conf. on Robotics and Automation, St. Louis, MO.* pp. 61–66.

Hanebeck, U. D. and G. Schmidt (1995). A New High Performance Multisonar System for Fast Mobile Robot Applications. In: *Intelligent Robots and Systems 1994 (IROS'94)* (V. Graefe, Ed.). pp. 1–14. Elsevier Science. Amsterdam.

Hanebeck, U. D. and G. Schmidt (1996). Set–theoretic Localization of Fast Mobile Robots Using an Angle Measurement Technique. In: *Proc. of the 1996 IEEE Int. Conf. on Robotics and Automation, Minneapolis, MN.* pp. 1387–1394.

Hanebeck, U. D., J. Horn and G. Schmidt (1996). On Combining Set–theoretic and Bayesian Estimation. In: *Proc. of the 1996 IEEE Int. Conf. on Robotics and Automation, Minneapolis, MN.* pp. 3081–3086.

Hofner, C. and G. Schmidt (1995). Path Planning and Guidance Techniques for an Autonomous Mobile Cleaning Robot. In: *Intelligent Robots and Systems 1994 (IROS'94)* (V. Graefe, Ed.). pp. 241–257. Elsevier Science. Amsterdam.

Nishizawa, T., A. Ohya and S. Yuta (1995). An Implementation of On–board Position Estimation for a Mobile Robot. In: *Proc. of the 1995 IEEE Int. Conf. on Robotics and Automation, Nagoya, Japan.* pp. 395–400.

Sabater, A. and F. Thomas (1991). Set Membership Approach to the Propagation of Uncertain Geometric Information. In: *Proc. of the 1991 IEEE Int. Conf. on Robotics and Automation, Sacramento, CA.* pp. 2718–2723.

Schweppe, F. C. (1973). *Uncertain Dynamic Systems.* Prentice–Hall.

Sutherland, K. T. and W. B. Thompson (1994). Localizing in Unstructured Environments: Dealing with the Errors. *IEEE Trans. on Robotics and Automation* **10**(6), 740–754.

Tsumura, T., H. Okubo and N. Komatsu (1993). A 3-D Position and Attitude Measurement System Using Laser Scanners and Corner Cubes. In: *Proc. of the 1993 IEEE/RSJ Int. Conf. on Intelligent Robots and Systems, Yokohama, Japan.* pp. 604–611.

Wiklund, U., U. Andersson and K. Hyyppä (1988). AGV Navigation by Angle Measurements. In: *Proc. of the 6th Int. Conf. on Automated Guided Vehicle Systems, Brussels, Belgium.* pp. 199–212.